# Natural Convection in a Vertical Porous Cavity Filled with a Non-Newtonian Binary Fluid

**Nabil Ben Khelifa**
Laboratoire des Technologies Innovantes, Université de Picardie Jules Vernes d'Amiens rue des Facultés le Bailly, 80025 Amiens Cedex, France

Laboratoire des Procédés Thermiques, Centre des Recherches et des Technologies de l'Energie, Technopole Borj Cedria B.P No 95, Hammam Lif 2050, Tunisie

**Zineddine Alloui**
Ecole Polytechnique, Université de Montréal, C.P. 6079, Succ. ''Centre Ville'', Montréal, QC H3C 3A7, Canada

**Hassen Beji**
Laboratoire des Technologies Innovantes, Université de Picardie Jules Vernes d'Amiens rue des Facultés le Bailly, 80025 Amiens Cedex, France

**Patrick Vasseur**
Laboratoire des Technologies Innovantes, Université de Picardie Jules Vernes d'Amiens rue des Facultés le Bailly, 80025 Amiens Cedex, France

Ecole Polytechnique, Université de Montréal, C.P. 6079, Succ. ''Centre Ville'', Montréal, QC H3C 3A7, Canada

*DOI 10.1002/aic.13815*
*Published online April 23, 2012 in Wiley Online Library (wileyonlinelibrary.com).*

*Numerical and analytical study of natural convection in a vertical porous cavity filled with a non-Newtonian binary fluid is presented. The density variation is taken into account by the Boussinesq approximation. A power-law model is used to characterize the non-Newtonian fluid behavior. Neumann boundary conditions for temperature are applied to the vertical walls of the enclosure, while the two horizontal ones are assumed impermeable and insulated. Both double-diffusive convection (*a = *0) and Soret-induced convection (*a = *1) are considered. Scale analysis is presented for the two extreme cases of heat-driven and solute-driven natural convection. For convection in a thin vertical layer (A* $\gg$ *1), a semianalytical solution for the stream function, temperature, and solute fields, Nusselt and Sherwood numbers are obtained using a parallel flow approximation in the core region of the cavity and an integral form of the energy and constituent equations. Numerical results of the full governing equations show the effects of the governing parameters, namely the thermal Rayleigh number,* $R_T$*, the Lewis number, Le, the buoyancy ratio,* $\varphi$*, the power-law index, n, and the integer number a. A good agreement between the analytical predictions and the numerical simulations is obtained.* © 2012 American Institute of Chemical Engineers *AIChE J,* 58: 1704–1716, 2012
*Keywords: non-Newtonian fluid, power-law model, porous media, binary solution*

## Introduction

Recently, the phenomenon of natural convection induced by two sources of buoyancy, through porous media, has been studied extensively due to its importance in many natural and industrial problems. These include petroleum extraction, underground diffusion of nuclear wastes and other contaminants, prevention of subsoil water pollution, porous material regenerative heat exchangers, solidification of binary mixtures, and so forth.

Available studies on natural convection in a binary fluid confined in a porous media are concerned mostly with the classical rectangular cavity heated from the vertical walls. Earlier studies on this topic are concerned with the so-called double-diffusive convection for which the solutal fields are induced by the imposition of given solutal boundary conditions along the vertical side walls. The pioneering investigation on this configuration seems to be due to Trevisan and Bejan[1] who investigated double-diffusive convection in a porous cavity with the two side walls maintained at different temperatures and solute concentrations. Both analytical and numerical results were reported by these authors. The same problem was also considered by Trevisan and Bejan[2] for the case of constant gradients of temperature and solute concentration applied on the vertical walls. Using numerical and analytical methods and scale analysis, this problem was re-examined for the cases of cooperative (Alavyoon[3]) and opposing (Alavyoon et al.[4]) constant fluxes of heat and mass imposed on the vertical walls. For opposing buoyancy forces, the possible existence of oscillating convection was

Correspondence concerning this article should be addressed to Z. Alloui at z.alloui@polymtl.ca.

demonstrated numerically by these authors. Also, for this situation, the existence of multiple solutions has been demonstrated analytically by Mamou et al.[5,6] The transition between aiding and opposing double-diffusive flows in a vertical porous cavity has been investigated by Amahmid et al.[7,8] It was demonstrated that two types of solutions exist in which thermal and solutal buoyancy forces oppose each other and are of comparable intensity. The special case for which the flow is driven by thermal and solutal buoyancy forces of equal and opposing intensity has been investigated by a few authors. For this situation, the rest state is a possible solution and convection occurs above a critical Rayleigh number. The onset of convection has been investigated by Mamou et al.[9,10] and Charrier-Mojtabi et al.,[11] on the basis of the linear stability theory, for the case of a cavity with the vertical walls kept at different but uniform temperatures and solute concentrations. The case of an inclined cavity has been considered by Mamou et al.[12] The critical stability limits were delineated in terms of the governing parameters of the problem. A numerical simulation of double-diffusive conjugate natural convection in an enclosure has been conducted by Kuznetsos and Sheremet.[13] The effects of finite thickness walls on the Nusselt and Sherwood numbers are discussed. A few studies have also be devoted to natural convection of a binary fluid induced by the phenomenon of thermal diffusion, also known as the Soret effect. For this situation, when a temperature gradient is applied to a binary mixture, initially homogeneous, thermal diffusion takes place, giving rise to a solutal gradient. Lorenz and Emery[14] investigated analytically the concentration field induced by the Soret effect in a vertical porous cavity heated isothermally from the sides. This theory was reconsidered by Dutrieux et al.[15] for the case of a porous medium modeled on the basis of the Brinkman equation. Chavepeyer and Platten[16] studied numerically the thermogravitational separation in a porous cavity saturated by a binary mixture. For random models of porous media, it was found that the Soret coefficient is independent of the presence of obstacles when considering a simple thermal diffusive regime. The onset of convection in a vertical porous medium, under the influence of the Soret effect, has been investigated by Marcoux et al.[17] for the particular situation where the buoyancy forces induced by the thermal and solutal forces are opposing and of equal intensity. The same problem has been reconsidered by Joly et al.[18] on the basis of Brinkman-extended Darcy model. An analytical solution for finite amplitude convection was found to be in good agreement with the numerical results obtained by these authors. Recently, convection in a horizontal porous enclosure heated and salted from the sides has been investigated by Er-Raki et al.[19] The influence of the Soret parameter on the onset of subcritical bifurcation was discussed by these authors. Mojtabi and coworkers[20] investigated the Soret-driven convection in a shallow porous horizontal slot submitted to a heat flux. The species separation between the two vertical ends of the cell was predicted in terms of the governing parameters of the problem.

In all the above studies, the binary solutions, saturating the porous media, are assumed to be Newtonian fluids. However, in many practical applications, the fluid is characterized by a complex rheological behavior such that a Newtonian assumption is inappropriate. Examples include petroleum drilling, chemical reactor design, polymer engineering, geophysical systems, certain separation processes, and so on. Despite this fact, studies focussing on natural convection in a porous cavity filled with a non-Newtonian binary fluid are only a few. A numerical and theoretical study of double-diffusive natural convection within a rectangular porous cavity saturated by a non-Newtonian fluid, and characterized by a power-law model, has been conducted by Getachew et al.[21] The order of magnitude predictions for the overall heat and mass transfer rates were demonstrated to be in good agreement with numerical results obtained by discrete numerical experiments. The case of a shallow cavity heated by constant heat and solute fluxes imposed across the vertical walls of enclosure has been investigated by Benhadji and Vasseur.[22] The problem was solved analytically, on the basis of the parallel flow approximation, in the limit of a thin layer. Solutions for the flow fields, Nusselt and Sherwood numbers are obtained in terms of the governing parameters of the problem. The effects of the Rayleigh and Lewis numbers, buoyancy ratio, and the power-law index of the fluid on the average Sherwood and Nusselt numbers are discussed by these authors.

This study focuses on natural convection problem inside vertical rectangular porous enclosure filled with a non-Newtonian binary fluid. The cavity is submitted to uniform heat fluxes from its vertical sides, while its horizontal boundaries are insulated and impermeable. The power-law model is adopted to characterize the non-Newtonian fluid behavior. The porous medium considered here is modeled according to the Darcy formulation. The differential equations describing the physical model are formulated in a standard manner assuming the validity of the Boussinesq approximation. The numerical and analytical results presented here are relevant to a better understanding of natural convection in a porous cavity filled with a non-Newtonian binary fluid.

## Problem Definition

The system under consideration is a two-dimensional cavity, filled with a porous medium saturated by a binary non-Newtonian fluid, of height $H'$ and width $L'$. The origin of the coordinate system is located at the center of the enclosure with $x'$, the horizontal axis, pointing to the right and $y'$, the vertical axis pointing in the opposite direction of the gravity force. A uniform constant heat and mass density of fluxes, $q'$ and $(1 - a)j'$, respectively, are applied along the two vertical walls. All the boundaries are hydrodynamically impermeable. The binary fluid is assumed to satisfy the Boussinesq approximation. The density variation with temperature and concentration is described by the state equation $\rho = \rho_0[1 - \beta'_T(T' - T'_0) - \beta_N(N - N_0)]$ where $\rho_0$ is the fluid mixture density at temperature $T' = T'_0$ and mass fraction of the reference component $N = N_0$, $\beta'_T$ and $\beta_N$ are the thermal and mass species expansion coefficients, respectively. The subscript o refers to condition at the origin of the coordinate system. The mass fraction of the denser component of the mixture, $N_0$, is assumed to be initially uniform.

The phenomenological equations relating the flux of heat $\vec{q}'$ and matter $\vec{j}'$ to the thermal and solute gradients present in a binary fluid mixture are given by (see for instance, De Groot and Mazur[23])

$$\vec{q}' = -k\nabla T' \tag{1}$$

$$\vec{j}' = -\rho D\nabla N - a\rho D' N_0 (1 - N_0)\nabla T' \tag{2}$$

where $a$ defines double-diffusive convection ($a = 0$) or Soret-induced convection ($a = 1$), $k$ and $D$ are the thermal

conductivity and the molecular (or isothermal) diffusion coefficient of species, and $D'$ is the thermodiffusion coefficient. The second term, in the right hand side of Eq. 2, describes the Soret effect, that is, mass separation due to a temperature gradient.

The non-Newtonian fluids considered here are those for which the rheological behavior can be described by the power-law model, proposed by Pascal,[24] whose expression, in term of apparent viscosity, is

$$\mu'_a = \varepsilon\left(u'^2 + v'^2\right)^{\frac{(n-1)}{2}} \varepsilon = \frac{2\mu'}{8^{(n+1)/2}(K'\phi)^{(n-1)/2}(n/(1+3n))^n} \tag{3}$$

where $K'$ and $\phi$ are the permeability and the porosity of the porous medium, respectively, $\mu'_a$ is the apparent viscosity, $\varepsilon$ is a parameter in power-law model, $\mu'$ is the consistency index, and $n$ is the power-law index. In the above model, the rheological parameters $\mu'$ and $n$ are assumed to be temperature independent.

The following dimensional variables (primed quantities are dimensional) are used

$$\begin{gathered}(x,y) = (x',y')/L' \quad (u,v) = (u',v')L'/\alpha \quad t = t'\alpha/(\sigma L'^2) \\ \Psi = \Psi'/\alpha \quad T = (T' - T'_0)/\Delta T' \quad \Delta T' = q'L'/k \\ S = N/\Delta N \quad \mu_a = \mu'_a/[\varepsilon(\alpha/L')^{n-1}]\end{gathered} \tag{4}$$

where $\Delta N = j'/\rho D$ for double-diffusive convection, $\Delta N = -N_0(1-N_0)\Delta T' D'/D$ for Soret-driven convection, and $\sigma = (\rho C)_p/(\rho C)_f$ is the heat capacity ratio.

Using the above equations, the dimensionless governing equations describing conservation of momentum, energy, and concentration are given as

$$\nabla^2\Psi = -\mu_a^{-1}\left[\frac{\partial\Psi}{\partial y}\frac{\partial\mu_a}{\partial y} + \frac{\partial\Psi}{\partial x}\frac{\partial\mu_a}{\partial x} + R_T\left(\frac{\partial T}{\partial x} + \varphi\frac{\partial S}{\partial x}\right)\right] \tag{5}$$

$$\left[\frac{\partial S}{\partial T} + \frac{\partial\Psi}{\partial y}\frac{\partial T}{\partial x} - \frac{\partial\Psi}{\partial x}\frac{\partial T}{\partial y}\right] = \nabla^2 T \tag{6}$$

$$\left[\frac{\partial S}{\partial t} + \frac{\partial\Psi}{\partial y}\frac{\partial S}{\partial x} - \frac{\partial\Psi}{\partial x}\frac{\partial S}{\partial y}\right] = \frac{1}{Le}\nabla^2 S \tag{7}$$

$$\mu_a = \left[\left(\frac{\partial\Psi}{\partial x}\right)^2 + \left(\frac{\partial\Psi}{\partial y}\right)^2\right]^{\frac{n-1}{2}} \tag{8}$$

where as usual, to satisfy the continuity equation, the stream function $\Psi$ is defined such that $u = \partial\Psi/\partial y$, $v = -\partial\Psi/\partial x$.

The nondimensional boundary conditions over the walls of the enclosure are

$$x = \pm\frac{1}{2}; \quad \Psi = 0; \quad \frac{\partial T}{\partial x} = 1; \quad \frac{\partial S}{\partial x} = (1-a) + a\frac{\partial T}{\partial x} \tag{9}$$

$$y = \pm\frac{A}{2}; \quad \Psi = 0; \quad \frac{\partial T}{\partial y} = 0; \quad \frac{\partial S}{\partial y} = 0 \tag{10}$$

where $A = H'/L'$ is the cavity aspect ratio.

In Eqs. 5–10, one must notice the presence of six dimensionless governing parameters, namely the modified thermal Rayleigh number $R_T$, the Lewis number $Le$, the buoyancy ratio $\varphi$, the power-law index $n$, the aspect ratio $A$, and constant $a$, defined as

$$\begin{gathered}R_T = K'\rho_0 g\beta'_T\Delta T'(L'/\alpha)^n/\varepsilon, \quad Le = \alpha/D \\ \varphi = \beta_N\Delta N/\beta'_T\Delta T', \quad A = H'/L'\end{gathered} \tag{11}$$

The heat and mass transfer rates, expressed in terms of the Nusselt and Sherwood numbers, respectively, can be computed from the following expressions

$$Nu = \frac{q'L'/\lambda}{\Delta T} = \frac{1}{T(1/2,0) - T(-1/2,0)} \tag{12}$$

$$Sh = \frac{j'L'/D}{\Delta S} = \frac{1}{S(1/2,0) - S(-1/2,0)} \tag{13}$$

where $\Delta T$ and $\Delta S$ are the side to side temperature and concentration differences, respectively. As $\Delta T$ and $\Delta S$ are $y$ independent, they are arbitrary evaluated at $y = 0$.

Equations 5–8, together with the boundary conditions 9 and 10 then completely determine the problem in terms of the governing parameters (Eq. 11). In the following sections, both analytical and numerical solutions are discussed.

## Numerical Solution

The solution of the governing equations 5–8 and boundary conditions 9 and 10 is obtained using a finite difference method with uniform grid size. The energy and the concentration equations were solved using the alternating direction implicit (ADI) method. The stream function field was solved using over relaxation method and known temperature and concentration distributions. A first-order backward finite difference scheme is used to discretize the temporal terms appearing in the governing equations. A line-by-line tridiagonal matrix algorithm with relaxation is used in conjunction with iterations to solve the nonlinear discretized equations. We consider that convergence is reached when $\Sigma_{i=1}^{m}(b_i^k - b_i^{k-1})/\Sigma_{i=1}^{m} b_i^k \leq 10^{-6}$ is satisfied, where $b$ stands for $\Psi$, $T$, and $S$. A further decrease of the convergence criteria $10^{-6}$ does not cause any significant change in the final results. Numerical tests have been performed to determine the minimum aspect ratio above which the flow can be assumed to be parallel. In the range of the parameters considered in this investigation, it was found that the numerical results can be considered independent of the aspect ratio when $A \geq 4$. For this reason, all the numerical results reported here were obtained for $A = 4$ with $60 \times 180$ mesh points.

Typical numerical results are presented in Figures 1a–c for different values of $n$, $R_T = 200$, $\varphi = 1$, $Le = 10$, $a = 0$ (double–diffusive driven convection). On the graphs, streamlines, isotherms, and isoconcentrates are presented from left to right. The numerically calculated maximum stream function ($\Psi_{\max}$), heat transfer ($Nu$), and mass transfer ($Sh$) are also given with each graph for reference. In these figures, the streamlines are equally spaced between $\Psi = 0$ on the boundaries and the maximum value $\Psi_{\max}$. Also, the isotherms are equally spaced between $T_{\max}$ and $T_{\min}$ and the isoconcentrates between $S_{\max}$ and $S_{\min}$. The case $n = 1$ corresponds to a Newtonian fluid for which, as illustrated in Figure 1b, the flow, temperature, and concentration fields are similar to those reported in literature by past investigations (see for instance Boutana et al.[25]). Figures 1a–c clearly illustrate the fact that for a tall cavity ($A \gg 1$), the flow in the core of the enclosure is essentially parallel, while the temperature and concentration are linearly stratified along the

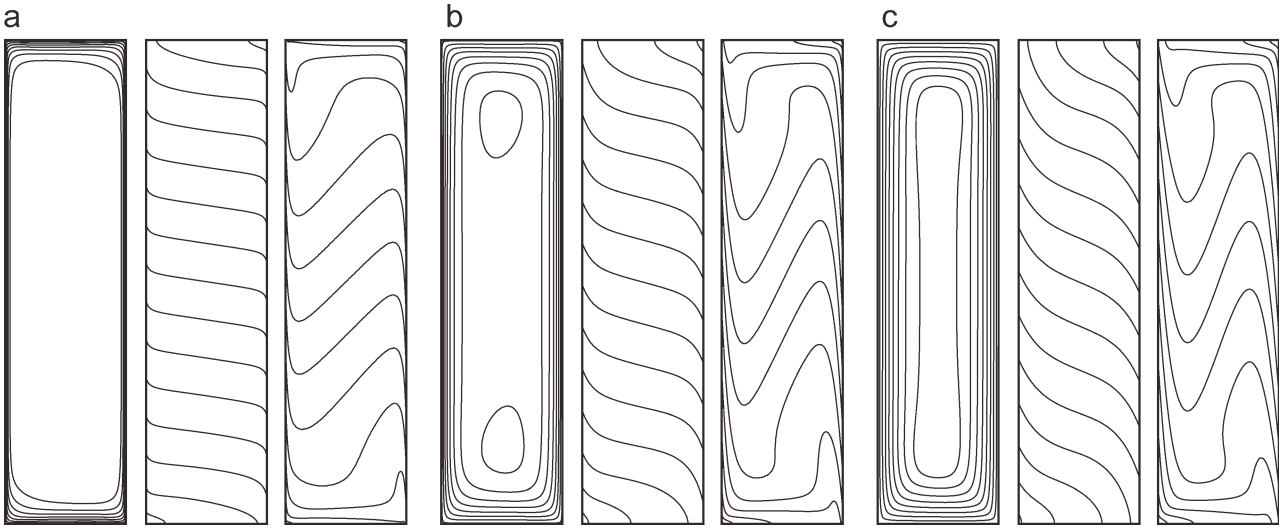


**Figure 1. Typical streamline (left), isotherm (center) and isoconcentration (right) patterns obtained numerically for $R_T = 200$, $\varphi = 1$, $Le = 10$, $a = 0$ and: (a) $n = 0.4$, $\Psi_{max} = 4.05$, $\Psi_{min} = 0$, $Nu = 12.53$, $Sh = 51.62$; (b) $n = 1$, $\Psi_{max} = 2.57$, $\Psi_{min} = 0$, $Nu = 4.18$, $Sh = 13.79$; (c) $n = 1.6$, $\Psi_{max} = 2.04$, $\Psi_{min} = 0$, $Nu = 2.53$, $Sh = 7.98$.**

vertical direction, and this independently of the values of power-law index $n$. This behavior is the base of the analytical model developed below.

## Parallel Flow Analysis

The approximate semianalytical solution is sought in the limit of a tall vertical cavity ($A \gg 1$). In the central part of the enclosure, the flow pattern can be assumed to be parallel in the $y$-direction, such that only the velocity component $v(x)$ in that direction exists.

As a result, the stream function, temperature, and concentration field must be, respectively, of the following form

$$\begin{aligned} \Psi(x,y) &\approx \Psi(x) \\ T(x,y) &\approx C_T y + \theta_T(x) \\ S(x,y) &\approx C_S y + \theta_S(x) \end{aligned} \tag{14}$$

where $C_T$ and $C_S$ are unknown constant temperature and concentration gradients in the $y$-direction, respectively. Substituting Eqs. 14 into Eqs. 5–7, one obtains the following system of ordinary differential equations

$$\frac{d}{dx}\left[\frac{d\Psi}{dx}\left|\frac{d\Psi}{dx}\right|^{n-1}\right] = -R_T \frac{d}{dx}(\theta_T + \varphi\theta_S) \tag{15}$$

$$\frac{\partial^2 \theta_T}{\partial x^2} = -C_T \frac{\partial \Psi}{\partial x} \tag{16}$$

$$\frac{\partial^2 \theta_S}{\partial x^2} = -(Le\, C_S + aC_T)\frac{\partial \Psi}{\partial x} \tag{17}$$

Only one half plane ($x > 0$) needs to be considered, because the core flow is cento symmetric about $x = 0$ and $y = 0$. Therefore, the above equations can be rewritten as

$$\frac{d\Psi}{dx} = -[R_T(\theta_T + \varphi\,\theta_S)]^{1/n} \quad \text{for} \quad \frac{d\Psi}{dx} < 0 \tag{18a}$$

$$\frac{d\Psi}{dx} = [-R_T(\theta_T + \varphi\,\theta_S)]^{1/n} \quad \text{for} \quad \frac{d\Psi}{dx} \geq 0 \tag{18b}$$

$$\frac{d^2\theta_T}{dx^2} = -C_T R_T^{1/n}(\theta_T + \varphi\,\theta_S)^{1/n} \tag{19}$$

$$\frac{d^2\theta_S}{dx^2} = -(Le\, C_S + aC_T)R_T^{1/n}(\theta_T + \varphi\,\theta_S)^{1/n} \tag{20}$$

subject to the following boundary conditions

$$x = 0 \;\; \frac{d\Psi}{dx} = 0; \quad \theta_T = 0; \quad \theta_S = 0 \tag{21}$$

$$x = \frac{1}{2} \;\; \Psi = 0; \quad \frac{d\theta_T}{dx} = 1; \quad \frac{d\theta_S}{dx} = (1-a) + a\frac{d\theta_T}{dx} \tag{22}$$

As discussed in the past by Bejan,[26] $C_T$ and $C_S$ may be obtained by considering an arbitrary control volume near the end regions of the cavity. Energy and solute balances, in this arbitrary control volume, are considered to find out the two constants. In this way, it can be easily demonstrated that the heat and solute transports across a transversal section, at any $y$, are given by the following expressions

$$\begin{aligned} &\int_{-1/2}^{1/2} \frac{\partial T}{\partial y}dx + \int_{-1/2}^{1/2} \frac{\partial \Psi}{\partial x} T dx = 0 \\ &\frac{1}{Le}\left(\int_{-1/2}^{1/2} \frac{\partial S}{\partial y}dx - a\int_{-1/2}^{1/2} \frac{\partial T}{\partial y}dx\right) + \int_{-1/2}^{1/2} \frac{\partial \Psi}{\partial x} S dx = 0 \end{aligned} \tag{23}$$

Substituting Eqs. 14 into Eqs. 23 and using the centrosymmetric conditions, one obtains

$$C_T = -2\int_0^{1/2} \frac{\partial \Psi}{\partial x}\theta_T\, dx \quad (C_S - aC_T) = -2\,Le \int_0^{1/2} \frac{\partial \Psi}{\partial x}\theta_S dx \tag{24}$$

By guessing the values of $C_T$ and $C_S$ and the temperature $\theta_T(x)$ and concentration $\theta_S(x)$ distributions, Eqs. 19, 20, and 24 together with boundary conditions, Eqs. 21 and 22, where solved iteratively using the Simpson integration scheme. To do so, Eqs. 19 and 20 were discretized using a finite difference procedure. The resulting equations were solved using an ADI method. The calculation was repeated until the convergence condition was met. The present semianalytical procedure is by far less time consuming that the numerical procedure involved in the solution of the full governing equations.

## Dimensional Analysis

In this section, order of magnitude estimates for the two limiting cases of heat-driven and solute-driven boundary layer type natural double-diffusive convection will be derived on the basis of scale analysis. The following derivations are based on the assumptions that $A \gg 1$ and that the flow has a boundary layer structure with a stratified core region (thermally and/or solutally).

### *Thermally driven boundary layer type convection*

When the buoyancy ratio is small ($\varphi \ll 1$), at sufficiently high thermal Rayleigh number $R_T$, the buoyancy forces that drive the fluid motion are mainly due to the temperature gradients. Let $\delta x$ be the thickness of the boundary layers, and $\delta v$, $\delta T$, and $\delta S$ be the velocity, temperature, and concentration changes across this layers. As a consequence of the thermal and solutal boundary conditions considered in this study, we have to deal with two different temperature scales. The first one is $\delta T$, the temperature variation across the vertical boundary layer. The second one is $\Delta T$, the temperature difference between the upper and the lower boundaries, which occurs over a length $A$. Thus, $C_T = \Delta T/A$ represents the thermal gradient within the core region of the cavity.

From the thermal boundary condition imposed along the vertical boundaries, Eqs. 9, it follows that

$$\frac{\delta T}{\delta x} \sim 1 \tag{25}$$

Applying the usual boundary layer approximation to Eqs. 5 and 6, the momentum and energy equations yield

$$\frac{\delta v^n}{\delta x} \sim R_T \frac{\delta T}{\delta x} \quad \text{and} \quad \delta v C_T \sim \frac{\delta T}{\delta x^2} \tag{26}$$

From the global balance of heat transport, Eq. 22, it follows that

$$\delta v \delta T \delta x \sim C_T \tag{27}$$

Solving Eqs. 25–27 then gives

$$\delta x \sim (R_T/n)^{-2/(3n+2)}, \quad \delta v \sim (R_T/n)^{3/(3n+2)}, \quad \delta \Psi \sim (R_T/n)^{1/(3n+2)}$$
$$\delta T \sim (R_T/n)^{-2/(3n+2)}, \quad C_T \sim (R_T/n)^{-1/(3n+2)} \tag{28}$$

From Eqs. 12 and 28, the Nusselt number is obtained as

$$Nu \sim (R_T/n)^{2/(3n+2)} \tag{29}$$

If the Rayleigh number $R_T$ is large enough, a boundary layer of thickness $\delta y$ will develop along the top and bottom boundaries of the cavity. Let $\delta u$ and $\overline{\delta T}$ be the velocity and temperature changes across this layer. From the conservation of mass it is found that

$$\delta u \delta y \sim \delta v \delta x \tag{30}$$

while the momentum Eq. 5 yields

$$\frac{\delta u^n}{\delta y} \sim R_T \delta T \tag{31}$$

Also, the conservation of energy (Eq. 23) requires that

$$\frac{\overline{\delta T}}{\delta y} \sim \delta v \delta T \delta x \tag{32}$$

Solving Eqs. 31–33, it is readily found that

$$\delta y \sim (R_T/n)^{-1/(3n+2)} \quad \delta u \sim (R_T/n)^{2/(3n+2)} \quad \overline{\delta T} \sim (R_T/n)^{-2/(3n+2)} \tag{33}$$

From the above results, it is clear that the vertical boundary layer is considerably thinner than the horizontal one. Also, the velocity and temperature changes across the vertical boundary layers are more important that the corresponding values in the horizontal boundary layers. On comparing Eqs. 28 and 33, it is observed that the dominating temperature change within the cavity is the one occurring in the thermally stratified core region, namely $\Delta T \sim A(R_T/n)^{-1/(3n+2)}$.

The concentration field convected by the flow induced by the temperature gradients will be now predicted for the two following limits:

### *Mass transfer rule by convection* $\mathbf{Le \gg 1}$

For this situation, as discussed by Alavyoon et al.,[3] due to the Neumann boundary conditions considered here the vertical concentration boundary layer has the same thickness as the hydrodynamic one, namely $\delta x$. Also, assuming that $\Delta S$ is the concentration difference between the upper and the lower boundaries, the concentration gradient within the core region is given by $C_S = \Delta S/A$.

From the vertical solutal boundary conditions, Eq. 9, considered in this study we have

$$\frac{\delta S}{\delta x} \sim 1 \tag{34}$$

The conservation of concentration, Eq. 17, requires that

$$\delta v C_S \sim Le^{-1} \frac{\delta S}{\delta x^2} \tag{35}$$

Substituting Eqs. 28 and 34 into Eq. 35 yields

$$C_S \sim Le^{-1}(R_T/n)^{-1/(3n+2)} \tag{36}$$

As $\delta S \sim \delta x \sim (R_T/n)^{-2/(3n+2)}$, it follows from Eq. 13 that the Sherwood number is of the order

$$Sh \sim (R_T/n)^{2/(3n+2)} \tag{37}$$

### *Mass transfer rule by convection* $\mathbf{Le \ll 1}$

For this situation, the horizontal profile of concentration is not of the boundary layer type, but rather, is diffusive. Thus, according to Eq. 23, it is readily found that

$$\delta v \delta x \sim Le^{-1} C_S \tag{38}$$

as the horizontal concentration drops over the width of the cavity is of $O(1)$. Substituting Eq. 28 into Eq. 38 yields

$$C_S \sim Le(R_T/n)^{1/(3n+2)} \tag{39}$$

while the Sherwood number for this diffusive situation is

$$Sh \sim 1 \tag{40}$$

***Solute-driven boundary layer type convection***

When the buoyancy ratio is sufficiently large ($\varphi \gg 1$), the buoyancy forces that drive the flow are mainly due to the gradient of concentration. Following the above procedure, the following scales are obtained

$$\begin{gathered}\delta x \sim (R_S/n)^{-2/(3n+2)} \quad \delta u \sim (R_S/n)^{2/(3n+2)} \quad \delta \psi \sim Le^{-1}(R_S/n)^{1/(3n+2)} \\ \delta S \sim (R_S/n)^{-2/(3n+2)} \quad C_S \sim (R_S/n)^{-1/(3n+2)} \quad Sh \sim (R_s/n)^{2/(3n+2)} \\ \delta y \sim (R_S/n)^{-1/(3n+2)} \quad \overline{\delta S} \sim (R_S/n)^{-2/(3n+2)} \quad \delta v \sim Le^{-1}(R_S/n)^{3/(3n+2)}\end{gathered} \tag{41}$$

where $R_S = \varphi Le R_T$ is the solutal Rayleigh number.

For $Le \gg 1$, that is, when the heat transfer is mainly by conduction, it is found that

$$C_T \sim Le^{-1}(R_S/n)^{1/(3n+2)} \tag{42}$$

and that

$$Nu \sim 1 \tag{43}$$

Similarly, for $Le \ll 1$, that is, when the heat transfer rate is due mainly by convection, one obtains

$$C_T \sim Le(R_S/n)^{-1/(3n+2)} \tag{44}$$

while $\delta T \sim \delta x$ such that the Nusselt number is given by

$$Nu \sim (R_T/n)^{2/(3n+1)} \tag{45}$$

## Results and Discussion

The effect of the governing parameters on the convective heat and mass transfers, as predicted by the present semianalytical solution, is now compared with the numerical results obtained by solving the full governing equations. As discussed above, for a tall cavity ($A \gg 1$), the governing parameters of the problem are the Rayleigh number $R_T$, buoyancy ratio $\varphi$, power-law index $n$, Lewis number $Le$, and parameter $a$. When the buoyancy ratio $\varphi$ is positive (negative), the solutal forces act in the same (opposite) direction than the thermal ones. The results reported in this study cover the range $10 \le R_T/n \le 10^3$; $-5 \le \varphi \le 10^2$; $10^{-2} \le Le \le 10^2$, and $0.2 \le n \le 1.8$.

Figures 2a–c illustrate the effects of the thermal Rayleigh number $R_T$ and power-law index $n$ on the strength of the convective motion, $\Psi_{max}$, and the heat and mass transfer, $Nu$ and $Sh$, respectively, for the case $Le = 10$, $\varphi = 0$, and $a = 0$. The semianalytical solution, displayed by solid lines, is seen to be in excellent agreement with the numerical solution of the full governing equations, depicted by small squares. Also depicted in the graphs are the predictions of

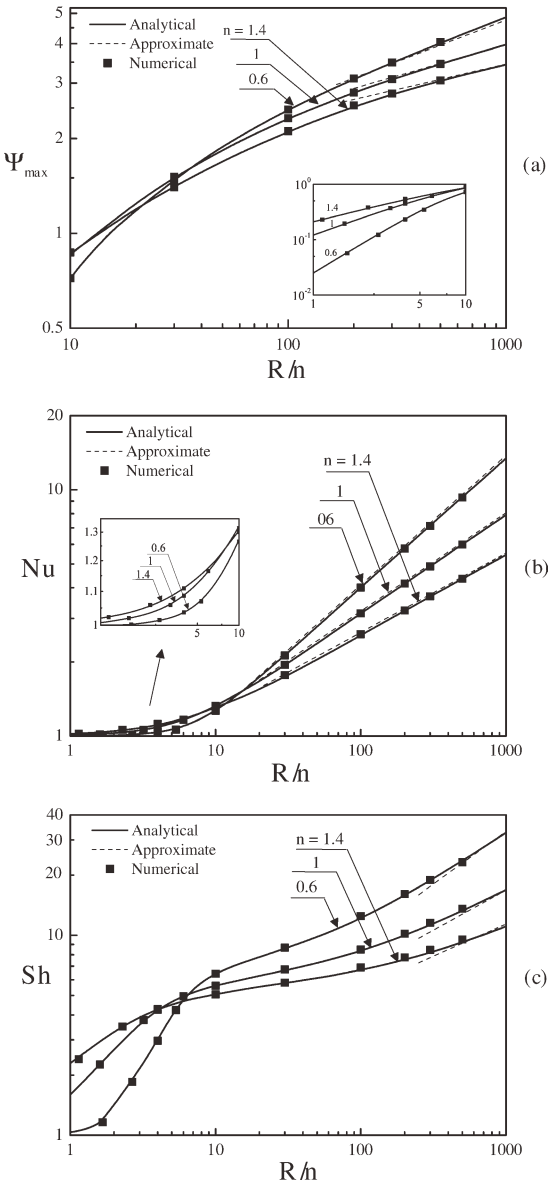


**Figure 2. The effects of the Rayleigh number $R_T$ and index $n$ in the power-law model on (a) maximum stream function $\Psi_{max}$, (b) heat transfer $Nu$, and (c) mass transfer $Sh$, for $Le = 10$, $\varphi = 0$, and $a = 0$.**

the scaling analysis. The averaged coefficients of the scale equations for the maximum stream function $\Psi_{max}$, Eq. 27, Nusselt number $Nu$, Eq. 29, and Sherwood number $Sh$, Eq. 37, which are only dependent of $n$, can be obtained from the predictions of the parallel flow analysis. In this way, they can be correlated into a function of $n$, in polynomial forms. Thus, for thermally driven boundary layer flow ($\varphi << 1$) and mass transfer rule by convection ($Le >> 1$), it is found that

$$\begin{aligned}\Psi_{max} &= [(1 + 4.2n - 1.2n^2)/4](R_T/n)^{1/(3n+2)} \\ Nu &= [(0.5 + 7n - 2n^2)/11](R_T/n)^{2/(3n+2)} \\ Sh &= [(8.7 + 9.5n - 1.2n^2)/16](R_T/n)^{2/(3n+2)}\end{aligned} \tag{46}$$

The above results are represented with dashed lines and it is seen that the present scaling analysis is reasonably correct. In general, Figure 2 indicates that, for a given value of $n$,

when $R_T$ is small enough, as expected convection is in the pseudoconduction regime such that $\Psi_{max} \to 0$, $Nu \to 1$, and $Sh \to 1$. On increasing the Rayleigh number, the strength of convection is promoted, such that the boundary layer regime is quickly reached. This occurs at approximately $R_T/n = 500$, almost independently of the value of $n$. Naturally, for a given value of the power-law index, the mass transfer is larger than the heat transfer as $Le$ is quite greater than unity, such that the mass diffusivity of the solution is smaller than the thermal one. Also, for a value of $R_T/n$ greater than about 10, Figure 2 shows that the strength of circulation and the convective heat and mass transfer rates are promoted on decreasing the power-law index $n$. However, it is noticed that for $R_T/n$ smaller than 10, this trend is reversed.

Figures 3a–c exemplify the effect of the buoyancy ratio $\varphi$ and power-law index $n$ on the strength of convection, $\Psi_{max}$, and heat and solute transfer rates, $Nu$ and $Sh$, respectively, for $R_T = 10^2$, $Le = 2$, and $a = 0$, that is, double-diffusive convection. Here, again the agreement between the semianalytical solution and the numerical results is found to be very good. As the buoyancy ratio $\varphi$ is positive, it follows that the thermal gradients and the solutal ones are coopering. The results indicates that, in the limit of $\varphi \to 0$, the convective motion within the cavity is driven solely by the thermal gradients. The resulting values of $\Psi_{max}$, $Nu$, and $Sh$, for a given $n$, are constants that depend of the values of the governing parameters considered here. On increasing the value of $\varphi$, the thermal regime is maintained up to about $\varphi \approx 0.5 \times 10^{-2}$ above which the combined effects of the thermal and solutal buoyancy forces enhance the strength of convection. Thus, above $\varphi \approx 1$, a sharp increase of $\Psi_{max}$, $Nu$, and $Sh$ with $\varphi$ is observed to occur. For $\varphi$ greater than a value that depends on $n$, the boundary layer is reached for which the curves tend toward straight lines. For a given value of $\varphi$, compared with the Newtonian fluids ($n = 1$), the strength of convection and the corresponding values of $Nu$ and $Sh$ are less (more) intense for larger (smaller) power-law index $n > 1$ ($n < 1$).

Figures 4a–c show the results obtained for the conditions of Figure 3, but for $a = 1$, that is, for Soret-induced convection. Naturally, in the limit of pure thermal convection ($\varphi \to 0$), the solution is the same as that reported above as for this situation the flow regime is independent of the solutal effects (i.e., $a$). On increasing the value of $\varphi$, the thermal regime is maintained up to about $\varphi \approx 0.1$ above which the strength of convection $\Psi_{max}$ and the Nusselt number drop sharply to reach constant values for $\varphi \geq 10$. This behavior, which is the opposite of the one reported above for double-diffusive convection, is due to the fact that as the value of $\varphi$ is increased, the numerical results (not presented here) indicate that the combined action of convection and the Soret effects give rise to a vertical stabilizing solutal gradient. Consequently, the convective motion within the cavity is drastically annihilated and the corresponding heat transfer reduced. To interpret the behavior of Figure 4c, it must be specified at this stage that the Sherwood number for $a = 1$ has not the same signification that for $a = 0$. For double diffusion, a flux of solute is imposed on the walls of the system such that for this situation, the Sherwood number has it usual meaning. However, for Soret-induced convection, the solid walls are impermeable to solute. Thus, the Sherwood number, as defined in Eq. 13, is merely an indication of the redistribution within the cavity, induced by the Soret effect and by convection, of the initially uniform concentration.

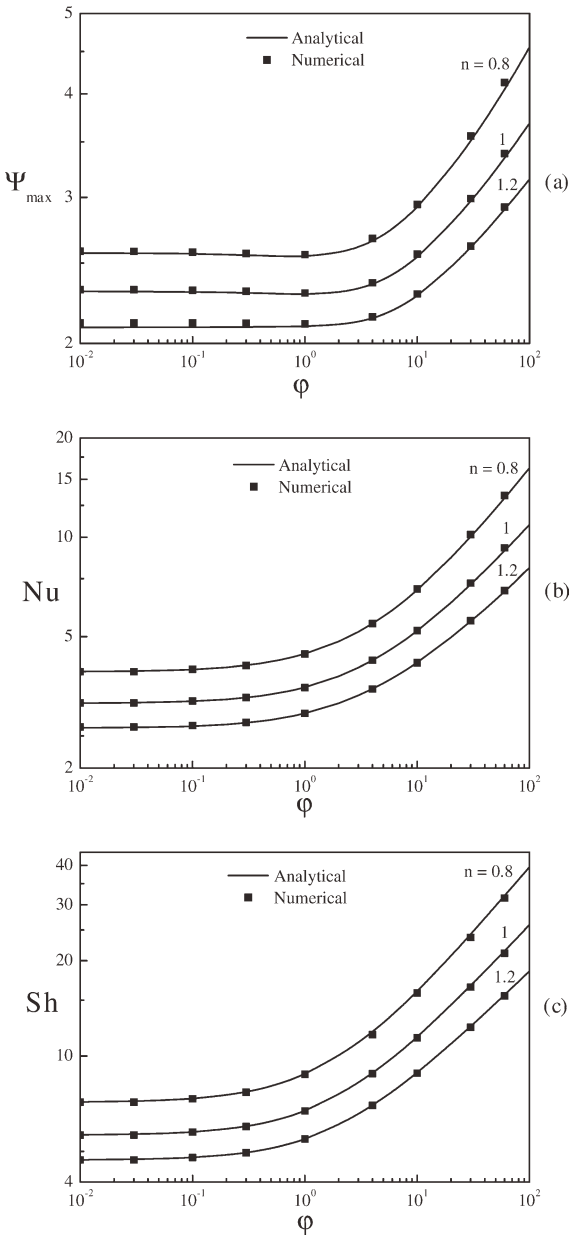


**Figure 3. The effects of the buoyancy ratio $\varphi$ and index in the power-law model $n$ on (a) maximum stream function, $\Psi_{max}$, (b) heat transfer, $Nu$, and (c) mass transfer, $Sh$, for $R_T = 100$, $Le = 2$, and $a = 0$.**

Figures 5 and 6 show the effects of $n$ on the vertical velocity, $v$, temperature, $T$, and concentration profiles, $S$, at the midheight horizontal section of the layer ($y = 0$), for $R_T = 200$, $\varphi = 1$, $Le = 2$, and $a = 0$ and 1, respectively. Here again, the excellent agreement between the solution of the semianalytical parallel flow analysis, depicted by solid lines, and the numerical results is observed. These profiles are antisymmetrical with respect to $x$ such that the results are presented only for $0 \leq x \leq 0.5$. As the porous medium is modeled according to Darcy's law, it is observed from Figures 5a and 6a that the velocity is maximum on the solid walls. This follows from the fact that, according to this model, the fluid is allowed to slip on a solid boundary. On increasing the power-law index $n$, it is seen that the velocity in the vicinity of the walls is considerably reduced, independently on

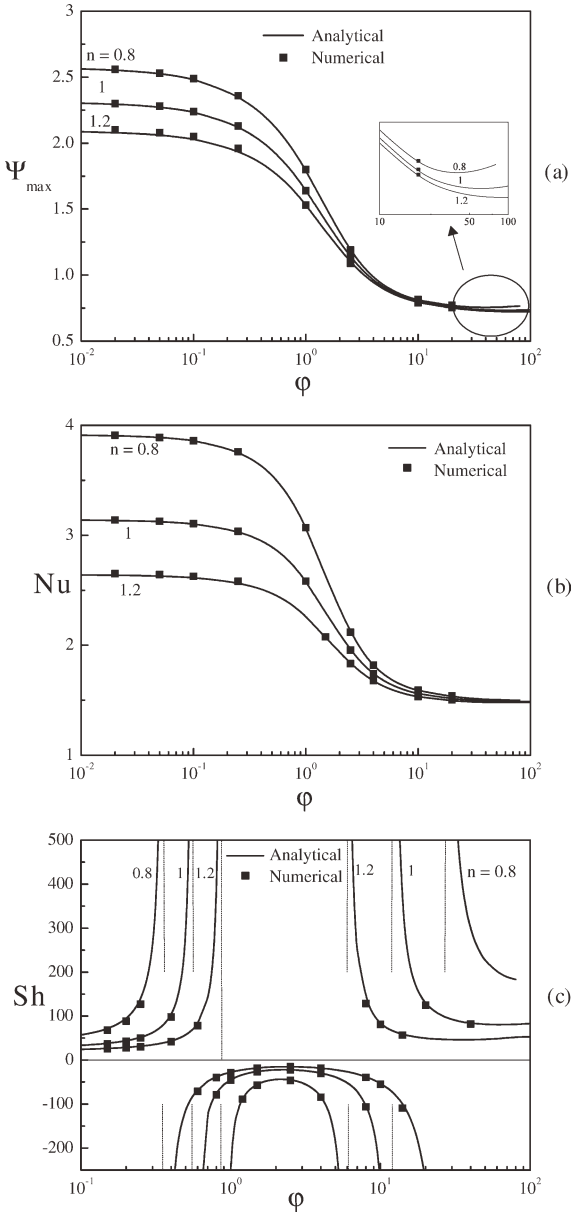


**Figure 4. The effects of the buoyancy ratio $\varphi$ and index in the power-law model $n$ on (a) maximum stream function, $\Psi_{max}$, (b) heat transfer, $Nu$, and (c) mass transfer, $Sh$, for $R_T$= 100, $Le$ = 2, and $a$ = 1.**

the value of $a$. According to Eq. 8, an increase of $n$ causes an increase of the apparent viscosity $\mu_a$, whose slowing down role on fluid motion is well-known. It results from what precedes that, in general, compared to Newtonian case ($n = 1$), the shear-thinning fluid ($0 < n < 1$) enhances the strength of circulation and the convective heat and mass transfer rates. On the other hand, the shear-thickening fluid ($n > 1$) produces an opposite effect. The effect of $n$ on the temperature profiles is illustrated in Figures 5b and 6b. An increase of $n$ reduces the intensity of convection resulting in an increase of the temperature on the walls so that the same heat flux can be maintained through the system. Concerning the concentration profiles, it is seen from Figure 5c that, in the case of double-diffusive convection, similarly to the temperature profiles, the concentration near the solid walls is promoted with an increase of the power-law index. However, for Soret-induced convection, the results are quite different as it can be seen from Figure 6c. As already discussed, for this situation, the concentration gradients does not result from the imposition of a constant heat mass flux on the solid walls but rather from a redistribution of initial uniform constant concentration within the system. As a result, the effect of $n$ on the concentration is relatively weak on the solid walls. Also, the vertical solutal gradient is observed to be stabilizing.

The effect of varying the Lewis number $Le$ and the power-law index $n$ on the strength of the convective motion, $\Psi_{max}$, and the heat and mass transfer $Nu$ and $Sh$ are presented in Figures 7a, b, respectively, for $R_T = 200$, $\varphi = 1$, and $a = 0$. Figure 7a indicates that, for small values of the Lewis number, the effect of the power-law index on the strength of convection is considerable. Thus, for $Le = 10^{-2}$,

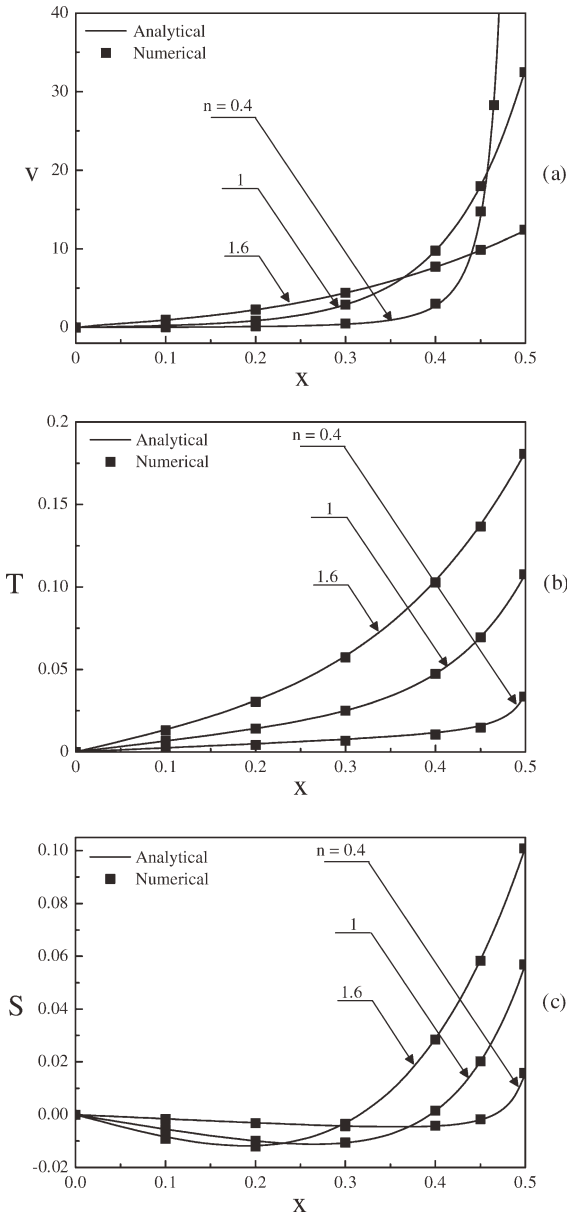


**Figure 5. The effects of the Rayleigh number $R_T$ and index in the power-law model $n$ on (a) velocity, (b) temperature, and (c) concentration profiles for $R_T$ = 200, $Le$ = 2, $\varphi$ = 1, and $a$ = 0.**

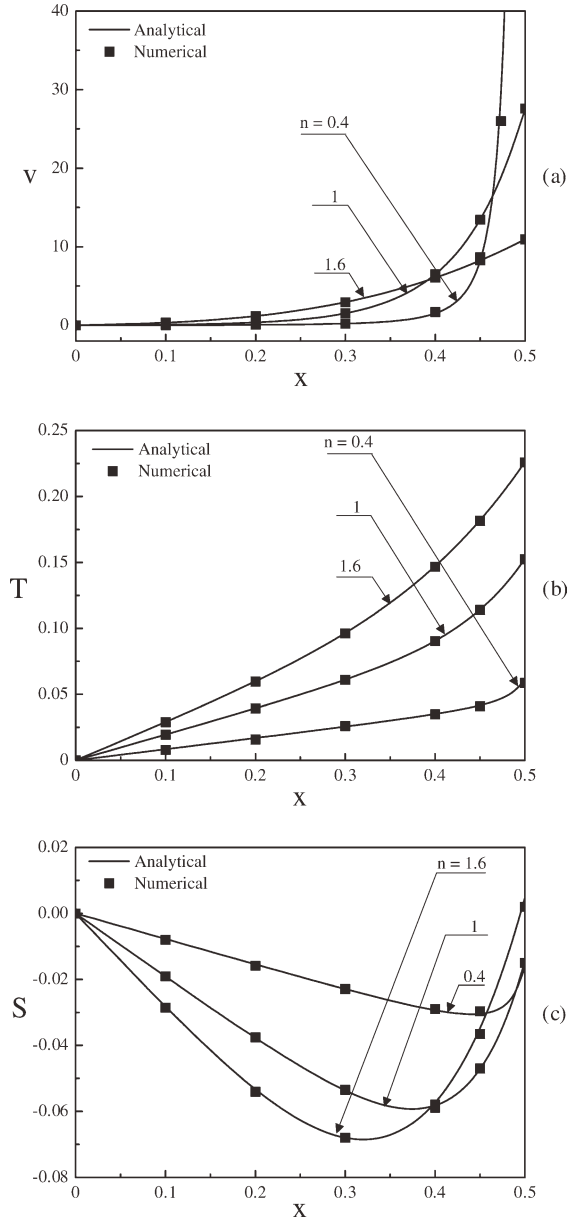


**Figure 6. The effects of the Rayleigh number $R_T$ and index in the power-law model $n$ on (a) velocity, (b) temperature, and (c) concentration profiles for $R_T = 200$, $Le = 2$, $\varphi = 1$, and $a = 1$.**

it is found that $\Psi_{max} = 50.34$ for $n = 1$ and $\Psi_{max} = 101.96$ (24.48) for $n = 0.8(1.2)$. As expected, when $Le \to 0$, Figure 7b reveals that the mass transfer is ruled by diffusion such that $Sh \to 1$, independently of the value of $n$. Similarly, the Nusselt number tends toward a constant that depends on the value of the power-law index. On increasing the value of the Lewis number, it is found that $\Psi_{max}$ decreases monotonously toward a constant value. Also, above $Le \approx 10$, it is seen that $\Psi_{max}$ becomes independent of the power-law index. On the other hand, the Sherwood number is considerably promoted on increasing $Le$ up to a value above which $Sh$ becomes independent of the Lewis number. For large values of $Le$, the influence $n$ on the Sherwood number is observed to be considerable. The effect of $Le$ on the Nusselt number is quite different. Thus, for small values of $Le$, $Nu$ is almost independent of the Lewis number. For intermediate values of $Le$ and a given value of $n$, $Nu$ is seen to increase first and then to decrease down to a constant value, for sufficiently large Lewis numbers.

Figure 8 illustrates the effects of the buoyancy ratio $\varphi$ and the power-law index $n$ on the strength of the convective motion $\Psi_{max}$, for $R_T = 20$, $Le = 10$, and $a = 0$. For this situation, the value of the buoyancy ratio is controlled by the strength of the solutal fluxes imposed on the vertical walls of the enclosure. The buoyancy ratio is varied in the range $-5$ to 5. This covers the spectrum from aided solutal-dominated flow ($\varphi = 5$), to purely thermal-dominated flow ($\varphi = 0$), to opposed but solutal-dominated flow ($\varphi = -5$). The case ($\varphi = -1$) corresponds to the particular situation where the buoyancy forced induced by the thermal and solutal effects is opposing each other and of equal intensity. For this situation, as discussed by many authors for the case of Newtonian fluids,[9–12,17,18] the rest state is a possible solution to the governing equations. However, convection may occur above a subcritical Rayleigh number $R_{TC}^{sub}$, the value of which depends on the governing parameters. In the present graph, the Rayleigh number considered is above the subcritical Rayleigh number such that $\Psi_{max} > 0$ when $\varphi = -1$. For a given value of $n$, Figure 8 indicates that when $\varphi$ is above zero, the thermal and solutal buoyancy forces act in the same direction (aiding flow) giving rise to a counterclockwise flow circulation ($\Psi_{max} > 0$). Increasing the buoyancy ratio from 0 to 5, the flow becomes more and more dominated by the mass species buoyant forces. When $\varphi$ is below zero, the thermal and solutal force act now in opposing

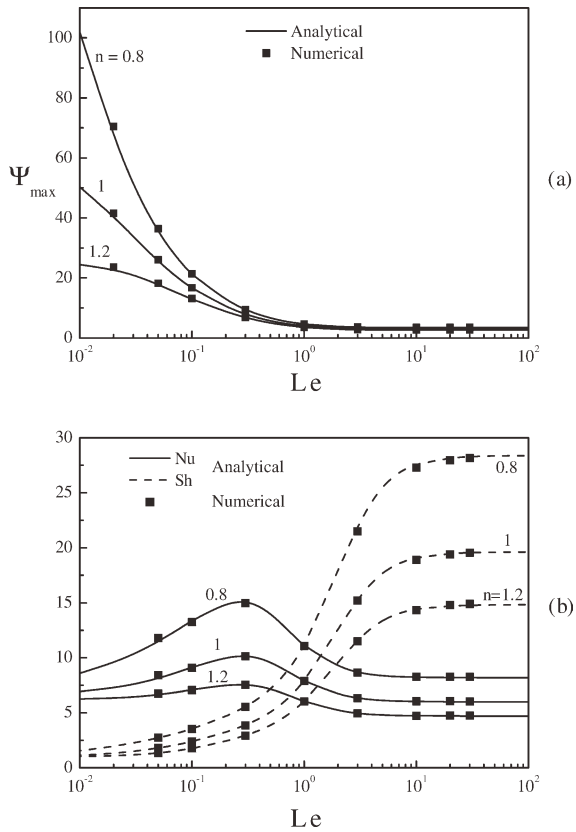


**Figure 7. The effects of the Lewis number $Le$ and index in the power-law model $n$ on (a) maximum stream function, $\Psi_{max}$, (b) heat and mass transfer, $Nu$ and $Sh$, for $R_T = 500$, $\varphi = 1$, and $a = 0$.**

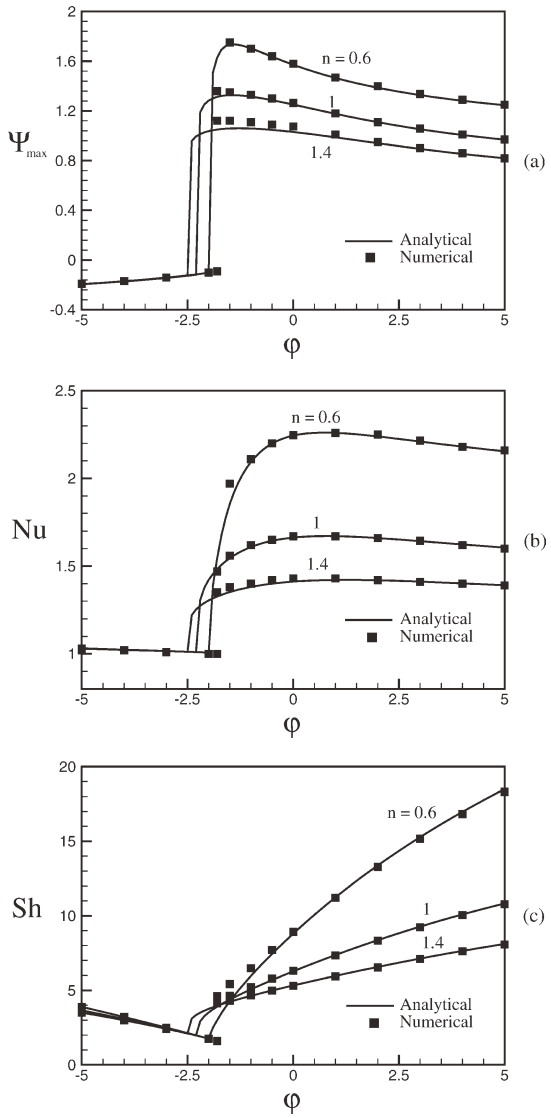


**Figure 8. The effects of the buoyancy ratio $\varphi$ and index in the power-law model $n$ on $\Psi_{max}$ for $R_T$ = 20, $Le$ = 10, and $a$ = 0.**

directions. In the range $-1 \leq \varphi \leq 0$, the thermal buoyancy forces are clearly dominating the flow such that $\Psi_{max}$ remains positive. Decreasing $\varphi$ further, it is expected that for sufficiently low values of this parameter, the flow circulation will become clockwise ($\Psi_{max} < 0$). The graph indicates that this occurs approximately at $\varphi \leq -1.75$ for the tree values of $n$ considered here.

The transition between the unicellular counterclockwise circulation and the unicellular clockwise circulation is illustrated in Figures 9 and 10 for the conditions of Figure 8 and $n$= 0.6 and 1.4, respectively. Because of the thermal and solutal conditions considered here the right side wall has a higher temperature and concentration than the left wall. As a result, the direction of the thermal flow is counterclockwise, whereas the direction of the solutal flow is clockwise (counterclockwise) for $\varphi \gg 0$ ($\varphi \ll 0$). Figure 9a shows the results obtained for a pseudoplastic fluid ($n = 0.6$), on decreasing $\varphi$ from zero to $-1.30$. The results indicate that the unicellular flow proceeds counterclockwise indicating that the thermal gradients, in the core of the cavity, are predominant over the opposing concentration ones. On decreasing the buoyancy ratio down to $\varphi = -1.76$, Figure 9b indicates that the flow consists now of a thermally driven counterclockwise rotating cell, in the central part of the cavity and two solutably driven clockwise circulations adjacent to the cavity walls. This result implies that the thermal buoyancy forces are still predominant even though the buoyancy ratio is relatively greater than unity. However, this situation is quite unstable, as on decreasing very slightly the buoyancy ratio down to $\varphi = -1.77$, one obtains the flow pattern depicted in Figure 9c. At this stage, a complete reversal of the direction of the flow is achieved. The numerical results indicate the existence of a unicellular motion rotating in the clockwise direction driven by solutal buoyancy. Similar results are presented in Figures 10a–c for a dilatant fluid ($n = 1.4$). The results are similar, but the zone of transition from unicellular counterclockwise thermally driven flow to unicellular clockwise solutally dominated circulation extends now from $-1.70 \leq \varphi \leq -1.92$.

Figure 11 illustrates the influence of the Rayleigh number $R_T$ and power-law index $n$ on $C_S$, the dimensionless solute

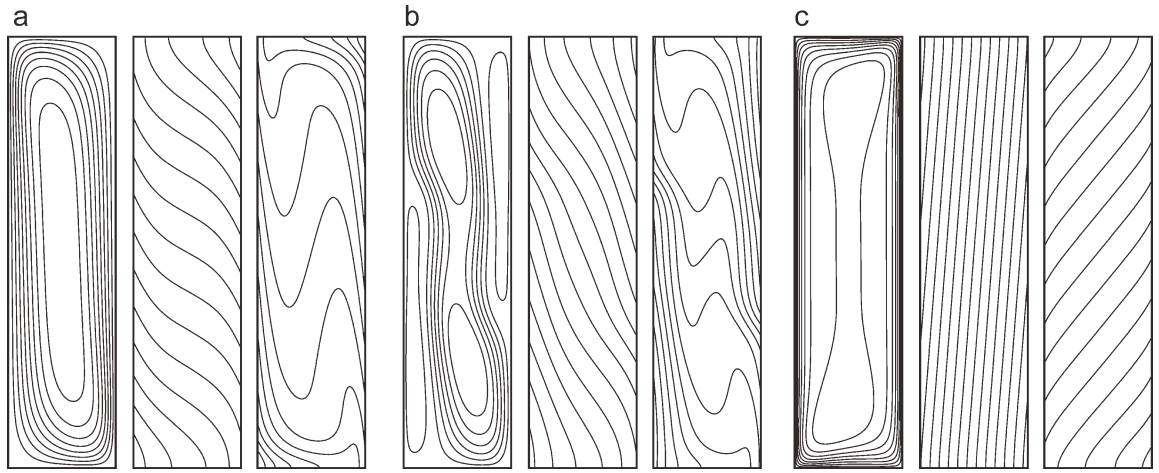


**Figure 9. Stream function, temperature, and concentration lines for the transition between thermal-dominated and solutal-dominated flows for $R_T$ = 20, $n$ = 0.6, $Le$ = 10, $a$ = 0 and: (a) $\varphi = -1.30$, $\Psi_{max} = 1.73$, $\Psi_{min} = 0$, $Nu$= 2.03, and $Sh$= 5.74; (b) $\varphi = -1.76$, $\Psi_{max} = -1.76$, $\Psi_{min} = -9.67\ 10^{-2}$, $Nu$= 1.13, and $Sh$= 1.73; (c) $\varphi = -1.77$, $\Psi_{max} = 0$, $\Psi_{min} = -9.74\ 10^{-2}$, $Nu$= 1.01, $Sh$= 1.58.**

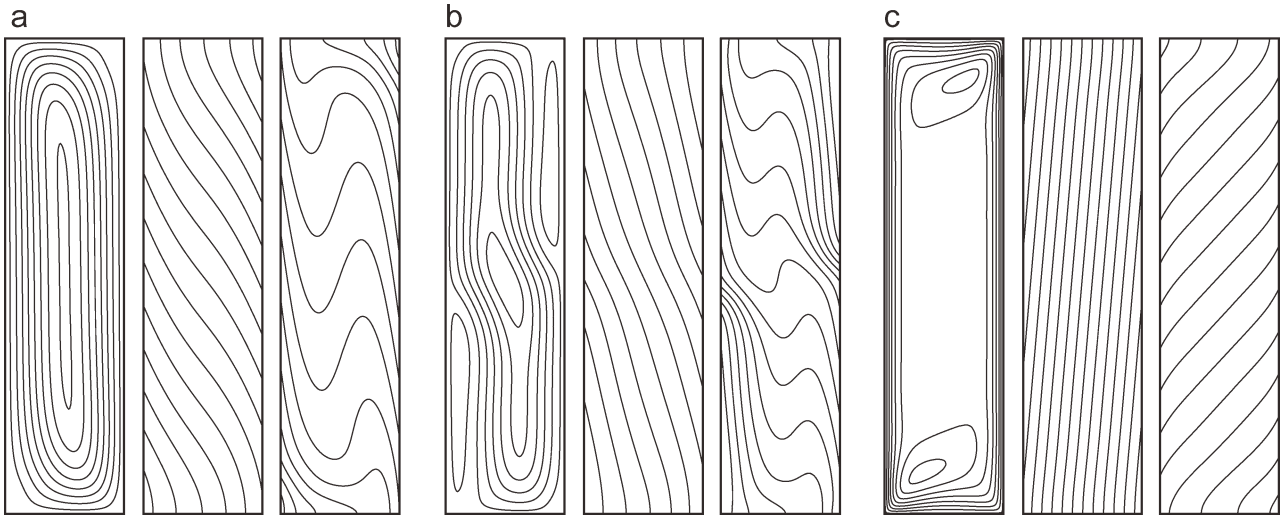


**Figure 10. Stream function, temperature, and concentration lines for the transition between thermal-dominated and solutal-dominated flows for $R_T = 20$, $n = 1.4$, $Le = 10$, $a = 0$, and: (a) $\varphi = -1.70$, $\Psi_{max} = 1.12$, $\Psi_{min} = -1.69\ 10^{-2}$, $Nu = 1.36$, and $Sh = 4.16$; (b) $\varphi = -1.90$, $\Psi_{max} = -0.92$, $\Psi_{min} = -0.14$, $Nu = 1.07$, $Sh = 3.13$; (c) $\varphi = -1.92$, $\Psi_{max} = 0$, $\Psi_{min} = -0.12$, $Nu = 1.01$, and $Sh = 1.7$.**

gradient in the vertical direction, for $Le = 10$, $\varphi = 0$, and $a = 1$. This gradient is a measure of the separation of the solute of the binary mixture, initially at uniform concentration. Thermal diffusion effect in columns differentially heated is a process that can be used in the industry of separation and as such has been recently the subject of a few investigations.[27–29] All these studies indicate the existence of an optimum separation condition that depends on the Rayleigh number, Lewis number, buoyancy ratio, type of thermal boundary conditions imposed on the system, inclination of the system, and so forth. However, up to now, only separations in Newtonian fluids have been considered. The results obtained here for such a fluid, $n = 1$, are qualitatively in agreement with what has been reported in the past. Thus, the graph indicates that there is a sharp maximum separation $C_s^{max}$ at an optimum value of the Rayleigh number $R_T^{opt}$. For $R_T \ll R_T^{opt}$, it is found that $C_S \rightarrow 0$ as the thermal diffusion (Soret effect) is predominant and the species migrate in a direction perpendicular to the thermally active walls. For $R_T \gg R_T^{opt}$, the results illustrate the fact that $C_S$ is also very small due to the intense mixing of the binary mixture resulting from the strong convective motion induced by the high Rayleigh number. For $R_T = R_T^{opt}$, the combined effects of thermodiffussion and convection yield a maximum separation for which $C_S = C_S^{max}$. The influence of power-law index $n$ on the separation process, namely $R_T^{opt}$ and $C_S^{max}$, is observed to be significant. Thus, it is found that, for a given set of the governing parameter, on decreasing (increasing) the value of $n$ below (above) unity, the optimum Rayleigh number $R_T^{opt}$ increases (decreases). Also, it is observed that a higher separation can be reached in the case of pseudoplastic fluids ($n < 1$) than dilatants ones ($n > 1$).

## Conclusions

Natural convection of a binary power-law fluid, in a tall vertical porous layer subject to horizontal gradients of temperature and solute, has been investigated both analytically and numerically. The modified Darcy model of Pascal[24] is used for the momentum equation. The influence of the thermal Rayleigh number $R_T$, buoyancy ratio $\varphi$, Lewis number $Le$, index parameter $n$, and parameter $a$, on the intensity of convection and heat and mass transfer, are predicted and discussed for a large range of the governing parameters. The summary of the major results is:

1. A scale analysis of the governing equations has been conducted to investigate the special cases of thermally driven ($\varphi << 1$) and solute-driven ($\varphi >> 1$) flow regimes. In the limit $\varphi \rightarrow 0$, the heat transfer is of the order $Nu \sim (R_T/n)^{2/(3n+2)}$, whereas the mass transfer is of order $Sh \sim (R_T/n)^{2/(3n+2)}$ when it is ruled by convection ($Le >> 1$) and of order 1 when it is ruled by conduction ($Le << 1$). When the Rayleigh number is high enough, for a boundary layer to develop along the top and bottom surfaces, the temperature difference between the horizontal boundaries is of the order $\Delta T \sim A(R_T/n)^{-1/(3n+2)}$ corresponding to a linear vertical stratification. On the other hand, in the limit $\varphi \rightarrow \infty$, the mass transfer is of the order $Sh \sim (R_S/n)^{2/(3n+2)}$, where $R_S = R_T \varphi Le$.

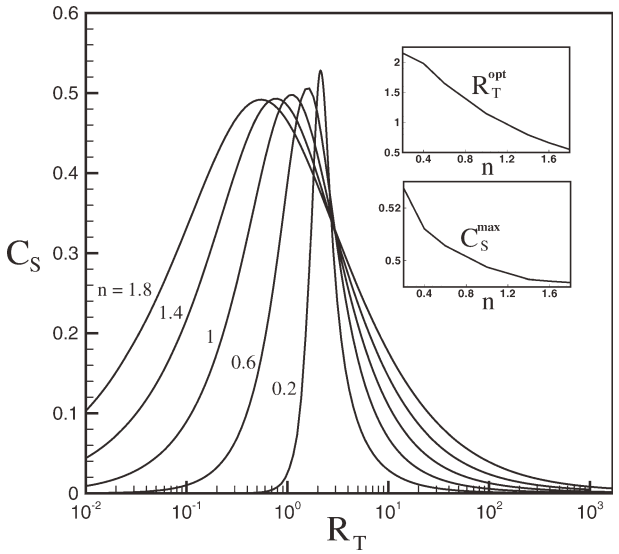


**Figure 11. The effects of the Rayleigh number $R_T$ and index in the power-law model $n$ on $C_S$ for $Le = 10$, $\varphi = 0$, and $a = 1$.**

2. The parallel flow approximation, valid in the limit of $A >> 1$, has been used to simplify the original set of governing partial differential equations. Although the resulting set of ordinary differential equations is considerably simpler, it has not been possible to obtain a closed form solution. Nevertheless, these equations have been solved numerically using a finite difference procedure. Although, the resulting semianalytical model requires a numerical procedure, this is by far a much easier task than solving numerically the original full set of governing equations.

3. The influence of the flow behavior index $n$ and the Rayleigh number $R_T$ on the fluid flow and heat and mass transfer rates has been demonstrated to be significant. Both the semianalytical and the numerical results indicate that there is a threshold parameter, $R_T/n$, the value of which depend of the governing parameters $\varphi$, $Le$, and $a$. Below this threshold, convection is relatively low and it is found that on increasing the value of $n$, the strength of circulation and the heat and mass transfers are enhanced. Above this threshold, the strength of convection is relatively high, this behavior is reversed. Most of the available results in literature are concerned with this last situation for which it is reported that, compare to Newtonian case ($n = 1$), the shear-thinning fluid ($0 < n < 1$) exhibits an enhancement of the strength of circulation and the convective heat and mass transfer rates while the shear-thickening fluid ($n > 1$) produces an opposite effect.

4. For negative values of the buoyancy ratio parameter, the range of the transition between the unicellular thermally induced circulation and the unicellular solutally induced circulation depends considerably upon the power-law index $n$ of the non-Newtonian binary solution.

5. The influence of power-law index $n$ on the separation process by the Soret effect of the solute in the binary solution is demonstrated to be significant. In particular, it is found that a higher separation can be reached in the case of shear-thinning fluids ($n < 1$) than shear-thickening ones ($n > 1$).

The main features, predicted by the semianalytical solution, were confirmed by numerical simulation of the full governing equations.

## Notation

$A$ = aspect ratio of the enclosure, $A = H'/L'$
$a$ = integer number
$C_S$ = dimensionless solute gradient in $y$-direction
$C_T$ = dimensionless temperature gradient in $y$-direction
$D$ = isothermal diffusion coefficient, $m^2/s$
$D'$ = thermodiffusion coefficient, $m^2/(s\ K)$
$g$ = gravitational acceleration, $m/s^2$
$H'$ = height of enclosure, m
$j'$ = constant solute flux per unit area, kg/(m s)
$k'$ = thermal conductivity, W/(m K)
$K'$ = permeability of porous medium, $m^2$
$L'$ = thickness of the enclosure, m
$Le$ = Lewis number, $\alpha/D$
$n$ = power-law index
$N$ = mass fraction of the reference component
$N_0$ = initial mass fraction of the reference component
$Nu$ = Nusselt number, Eq. 12
$q'$ = constant heat flux per unit area, $W/m^2$
$R_T$ = thermal Rayleigh number, $K'\rho_0 g\beta'_T\Delta T'(L'/\alpha)^n/\varepsilon$
$S$ = normalized mass fraction, $N/\Delta N$
$Sh$ = Sherwood number, Eq. 13
$\Delta S$ = characteristic mass fraction difference of the reference component
$T$ = dimensionless temperature
$\Delta T$ = characteristic temperature difference, $q'L'/k$
$u$ = dimensionless velocity $x$-component
$v$ = dimensionless velocity $y$-component
$x, y$ = Cartesian coordinates measured from the center of cavity

### Greek letters

$\alpha$ = fluid thermal diffusivity, $m^2/s$
$\beta_N$ = mass species expansion coefficient
$\beta_{T'}$ = thermal expansion coefficient, $K^{-1}$
$\Psi$ = dimensionless stream function, $\Psi'/\alpha$
$\rho$ = density of fluid, $kg/m^3$
$\varepsilon$ = parameter in power-law model, $Pa\ s^n/m^{n-1}$
$\phi$ = porosity of the porous medium
$\varphi$ = buoyancy ratio, $\beta_N\Delta N/\beta'_T\Delta T'$
$\mu_a'$ = apparent viscosity in power-law model, $Pa\ s^{n-1}$
$\mu'$ = consistency index, $Pa\ s^n$
$\xi$ = normalized porosity of the porous medium, $\phi/\sigma$

### Superscript

$'$ = dimensional quantities

### Subscripts

$o$ = refers to the value taken at the centre of the cavity
$c$ = refers to critical conditions

## Literature Cited


1. Trevisan O, Bejan A. Natural convection with combined heat and mass transfer. *Int J Heat Mass Transfer*. 1985;28:1597–1611.
2. Trevisan O, Bejan A. Mass and heat transfer by natural convection in a vertical slot filled with porous medium. *Int J Heat Mass Transfer*. 1986;29:403–415.
3. Alavyoon F. On natural convection in vertical porous enclosures due to prescribed fluxes of heat and mass at the vertical boundaries. *Int J Heat Mass Transfer*. 1993;36:2479–2498.
4. Alavyoon F, Masuda Y, Kimura S. On natural convection in vertical porous enclosures due to opposing fluxes of heat and mass prescribed at the vertical walls. *Int J Heat Mass Transfer*. 1994;37:195–206.
5. Mamou M, Vasseur P, Bilgen E, Gobin D. Double-diffusive convection in an inclined slot filled with porous medium. *Eur J Mech B/fluids*. 1995;14:629–652.
6. Mamou M, Vasseur P, Bilgen E. Multiple solutions for double diffusive convection in a vertical porous enclosure. *Int J Heat Mass Transfer*. 1995;38:1787–1798.
7. Amahmid A, Hasnaoui M, Mamou M, Vasseur P. On the transition between aiding and opposing double diffusive flows in a vertical porous matrix. *J Porous Media*. 2000;3:123–137.
8. Amahmid A, Hasnaoui M, Mamou M, Vasseur P. Boundary layer flows in vertical porous enclosures induced by opposing buoyancy forces. *Int J Heat Mass Transfer*. 1999;42:3599–3608.
9. Mamou M, Hasnaoui M, Amahmid A, Vasseur P. Stability of double diffusive convection in a vertical Brinkman porous enclosure. *Int Comm Heat Mass Transfer*. 1998;25:491–500.
10. Mamou M, Vasseur P, Bilgen E. Double-diffusive convection instability in a vertical porous enclosure. *J Fluid Mech*. 1998;368:263–289.
11. Charrier-Mojtabi MC, Karimi-Fard M, Azaiez M, Mojtabi A. Onset of a double-diffusive convection regime in a rectangular cavity. *J Porous Media*. 1998;1:107–121.
12. Mamou M, Vasseur P, Bilgen E. A Galerkin finite element study of the onset of double-diffusive convection in an inclined porous enclosure. *Int J Heat Mass Transfer*. 1998;41:1513–1529.
13. Kuznetsos GV, Sheremet M. A numerical simulation of double-diffusive conjugate natural convection in an enclosure. *Int J Therm Sci*. 2011;50:1878–1886.
14. Lorenz M, Emery AH. The packed thermal diffusion column. *Chem Eng Sci*. 1959;11:16–23.
15. Dutrieux JF, Chavepeyer G, Platten JK, Itasse E. La théorie de Lorenz-Emery revisitée: influence des bords. *Entropie*. 1999;218:18–21.
16. Chavepeyer G, Platten JK. Approche de la séparation thermogravitationelle d'un liquide binaire en modèle aléatoire de milieux poreux par moyennes d'ensembles. *Entropie*. 1998;214:27–30.
17. Marcoux M, Charrier-Mojtabi MC, Bergeron A. Naissance de la thermogravitation dans un mélange binaire imprégnant un milieu poreux. *Entropie*. 1998;214:31–36.
18. Joly F, Vasseur P, Labrosse G. Soret instability in a vertical Brinkman porous enclosure. *Numer Heat Transfer*. 2001;39:339–359.
19. Er-Raki M, Hasnaoui M, Amahmid A, Bourich M. Subcritical convection in the presence of Soret effect within a horizontal porous

enclosure heated and salted from the short sides. *Int J Numer Methods Heat Fluid Flow*. 2011;21:150–167.
20. Charrier-Mojtabi MC, Elhajjar B, Ouattara B, Mojtabi A, Costeséque P. Soret-driven convection and separation of binary mixtures in a porous horizontal slot submitted to a heat flux. *CR Mecanique*. 2011;339:303–309.
21. Getachew D, Poulikakos D, Minkowycz J. Double diffusion in a porous cavity saturated with a non-Newtonian fluid. *J Thermophys Heat Transfer*. 1998;38:437–446.
22. Benhadji K, Vasseur P. Double diffusive convection in a shallow porous cavity filled with a non-Newtonian fluid. *Int Comm Heat Mass Transfer*. 2001;28:763–772.
23. De Groot SR, Mazur P. *Non Equilibrium Thermodynamics*. Amsterdam: North Holland Pub, 1969.
24. Pascal H. Rheological behaviour effect of non-Newtonian fluids on steady and unsteady flow through porous media. *Int J Numer Anal Methods Geomech*. 1983;7:207–224.
25. Boutana N, Bahloul A, Vasseur P, Joly F. Soret-driven and double-diffusive natural convection in a vertical porous cavity. *J Porous Media*. 2004;7:1–17.
26. Bejan A. The boundary layer regime in a porous layer with uniform heat flux from side. *Int J Heat Mass Transfer*. 1983;26:1339–1346.
27. Estbe J, Schott J. Concentration saline et cristallisation du milieu poreux par effet thermogravitationnel. *CR Acad Sci Paris*. 1970;Serie IIb:805–807.
28. Marcoux M, Charrier-Mojtabi MC. Naissance de la convection thermosolutale dans une cellule rectangulaire poreuse soumise à des flux de chaleur et de masse. *Entropie*. 1999;218:8–12.
29. Bahloul A, Yahiaoui MA, Vasseur P, Robillard L. Thermogravitational separation in a vertical annular porous layer. *Int Comm Heat Mass Transfer*. 2004;31:783–794.

*Manuscript received Feb. 2, 2012, and revision received Mar. 22, 2012.*